Journal of Hazardous Materials 179 (2010) 251–257

Contents lists available at ScienceDirect

Journal of Hazardous Materials

journal homepage: www.elsevier.com/locate/jhazmat

A novel magnetically separable γ-Fe_2O_3/crosslinked chitosan adsorbent: Preparation, characterization and adsorption application for removal of hazardous azo dye

Hua-Yue Zhu[a,b], Ru Jiang[a], Ling Xiao[b,*], Wei Li[b]

[a] Department of Environmental Engineering, Taizhou University, Linhai 317000, PR China
[b] College of Resource and Environmental Science, Hubei Biomass-Resource Chemistry and Environmental Biotechnology Key Laboratory, Wuhan University, Wuhan 430072, PR China

ARTICLE INFO

Article history:
Received 8 November 2009
Received in revised form 25 February 2010
Accepted 25 February 2010
Available online 3 March 2010

Keywords:
Chitosan
Methyl orange
γ-Fe_2O_3
Magnetic separation
Adsorption

ABSTRACT

A novel magnetically separable adsorbent, namely magnetic γ-Fe_2O_3/crosslinked chitosan composites (Mγ-Fe_2O_3/CSCs), was prepared by miroemulsion process and characterized by XRD, FT-IR, TGA, DSC, SEM and VSM. Adsorption of methyl orange (MO), used as a model pollutant, from aqueous solution on Mγ-Fe_2O_3/CSCs was investigated. Characterization results indicated that magnetic γ-Fe_2O_3 nanoparticles have been introduced in Mγ-Fe_2O_3/CSCs and kept intrinsic magnetic properties. The saturated magnetization (σ_s) of Mγ-Fe_2O_3/CSCs can be expediently adjusted by changing additive dosage of γ-Fe_2O_3. Adsorption results showed that both nanocomposite adsorbents with weight ratio of γ-Fe_2O_3 to chitosan of 1:10 and 2:5 exhibited higher adsorption capacities and attained adsorption equilibriums in shorter time compared with crosslinked chitosan. After adsorption, Mγ-Fe_2O_3/CSCs were effectively separated from reaction solution in 10 s by applying an adscititious magnetic field. Adsorption kinetics of MO on 1:10 Mγ-Fe_2O_3/CSCs followed the pseudo-second-order kinetic model. Effects of both initial pH and adsorbent dosage on the adsorption of MO were remarkable in experimental conditions.

1. Introduction

Azo dyes are characterized by the presence of N=N group and widely used in dyeing textile, leather, cosmetics, ink, food processing [1,2]. However, about 15% of dyes produced are lost during dyeing processes and released into wastewaters. Due to large degree of aromatics present in azo dye molecules and their biological persistence, conventional biological treatment methods are often ineffective for hazardous azo dye decolorization and removal [3]. At the same time, these dyes can cause irreversible damages to environment, aquicolous organisms and human health. In recent years, numerous treatment methods, including coagulation, flocculation, heterogeneous photocatalysis and membrane filtration, have been used to decolorize dye effluents [4–7]. All these processes have their own limitations, such as sludge generation, formation of aromatic amines and membrane fouling, etc. Adsorption on solid surface is being grown interest in wastewater treatment and considered as an efficient and economical method to remove dyes from aqueous solutions [3,8–13].

Chitosan is a deacetylated product of chitin, naturally occurring biopolymer, which is the second most abundant polysaccharid in the world after cellulose. Raw, grafted and crosslinked chitosans used as economical adsorbents are drawing great attention and showing significant adsorption potential for removal of various dyes since amino(–NH_2) and hydroxy (–OH) functional groups on chitosan chains can serve as electrostatic interaction and coordination bonds, respectively [10–13]. However, the difficulty in separating those powdery chitosan-based adsorbents, except high speed centrifugation, from treated effluent limits their practical applications. Magnetic assisted adsorption separation technology provides an alternative method to separate powdery adsorbents from solution effectively [14–16]. Magnetic adsorbents can be used to adsorb contaminants from aqueous solutions and easily separated or recovered from the medium by a simple magnetic process after adsorption [16,17]. Magnetite (Fe_3O_4) and maghemite (γ-Fe_2O_3) have been widely used as magnetic material due to their excellent magnetic properties, chemical stability and biocompatibility [15,16,18–22]. Recently, many researches have reported about magnetic chitosan/Fe_3O_4 composites and their applications in removal of metal ions, adsorption of *Saccharomyces cerevisiae* and mensuration of ferritin [18–22]. However, to our knowledge, there have been no reports on preparation, characterization and adsorption

* Corresponding author at: Luojia Mountain of Wuchang, Wuhan City, Hubei Province, 430072, PR China. Tel.: +86 027 61063891.
E-mail address: xiaoling9119@yahoo.cn (L. Xiao).

0304-3894/$ – see front matter © 2010 Elsevier B.V. All rights reserved.
doi:10.1016/j.jhazmat.2010.02.087

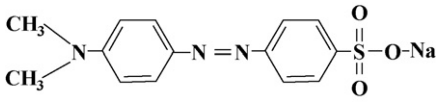

Fig. 1. Chemical structure of methyl orange.

properties of magnetic nanosized γ-Fe_2O_3/chitosan composite adsorbent.

In this paper, magnetic γ-Fe_2O_3/crosslinked chitosan composites (Mγ-Fe_2O_3/CSCs) were prepared by microemulsion process using magnetic γ-Fe_2O_3 nanoparticles as magnetic material and chitosan as basic adsorbent, then characterized by XRD, FT-IR, TGA, DSC, SEM and VSM. A typical azo dye, namely methyl orange (MO), was used as a model azo dye to investigate adsorption properties of Mγ-Fe_2O_3/CSCs by batch adsorption experiments. Effects of both initial solution pH and adsorbent dosage on dynamic behavior of adsorption were examined. Adsorption kinetics was evaluated with Lagergren-first-order, pseudo-second-order and intraparticle diffusion kinetic models. This information may be useful for further application for the system design in removal of hazardous azo dyes from aqueous solution.

2. Experimental

2.1. Chemicals and materials

Chitosan (CS, MW 2.1×10^5 g mol^{-1}; degree of deacetylation 91.7%) was purchased from Zhejiang Yuhuan Ocean Biology Co., Ltd (Taizhou, China). Commercially available magnetic γ-Fe_2O_3 (20–30 nm outer diameters; 98% purity) was obtained from Tongrenweiye Technology Co., Ltd (Shijiazhuang, China). Methyl orange (C.I. acid orange 52; $C_{14}H_{14}N_3SO_3Na$; MW 327.33 g mol^{-1}) was purchased from Yongjia Fine Chemical Factory (Wenzhou, China). Fig. 1 displays the chemical structure of methyl orange. Other chemicals were of analytical grade and used without any further purification. All solutions were prepared by double distilled water.

2.2. Preparation of Mγ-Fe_2O_3/CSCs

Details in the preparation procedures of Mγ-Fe_2O_3/CSCs were described as follows: 0.5 g chitosan was dissolved in 20 mL 2% (v/v) of acetic acid aqueous solution. Then magnetic γ-Fe_2O_3 nanoparticles were dispersed uniformly into the colloidal solution under ultrasonic stirring for 30 min. Subsequently, dispersion medium composed of 80 mL paraffin and 4 mL emulsifier (Span-80) was poured into the mixed system under mechanical stirring at room temperature. After 30 min, 2 mL glutaraldehyde (25%, v/v) was dropped slowly into the reaction system and stirred in a water bath at 40 °C for 60 min. pH of reaction solution was adjusted to 9–10 by using 1 mol L^{-1} NaOH and kept at 70 ± 0.2 °C for a further 60 min. The products were then collected by the aid of an adscititious magnet and washed with N, N-dimethylformamide, ethanol and distilled water for three times, respectively. Finally, the brown products (Mγ-Fe_2O_3/CSCs) were dried in an oven at 60 °C under atmospheric condition. According to weight ratio of magnetic γ-Fe_2O_3 nanoaprticles to chitosan, two products were named as 1:10 Mγ-Fe_2O_3/CSCs and 2:5 Mγ-Fe_2O_3/CSCs, respectively.

Chitosan particles were prepared in the same procedure but no addition of γ-Fe_2O_3.

2.3. Characterization of Mγ-Fe_2O_3/CSCs

Crystal structures of samples were determined by performing X-ray diffraction (XRD) on D8 ADVANCE X-ray diffraction spectrometer (Bruker, German) with a Cu Kα target at 40 kV and 50 mA at a scan rate of 2° 2θ min^{-1}. Micro-structures of samples were observed by scanning electron microscopy (SEM) with a Hitachi SX-650 machine (Tokyo, Japan). Fourier transform infrared (FT-IR) spectra were measured at room temperature on a FT-IR-8400 spectrometer (Shimadzu, Japan). Thermogravimetric analyses (TGA) and differential scanning calorimetry (DSC) of samples were performed in a Setaram Setsys 16 TG/DTA/DSC (France) under a nitrogen atmosphere of 0.15 MPa from 25 °C to 800 °C with a heating rate of 2 °C min^{-1}. Magnetic hysteresis loops were obtained at room temperature using a HH-15 model vibrating sample magnetometer (VSM) (Nanjing University, China). An IXUS 95 IS digital Cannon camera (Japan) was used to take photos of solution before and after magnetic separation.

2.4. Batch adsorption experiments

Adsorption of MO on Mγ-Fe_2O_3/CSCs was studied by batch experiments. A stock solution (1.0 g L^{-1}) of MO was prepared from analytical-reagent product. The stock solution was then diluted to give a series of standard solutions in different concentrations. Batch adsorption experiments were carried out using a model KYC-1102C thermostated shaker (Ningbo Jiangnan Instrument Factory, China) at 100 rpm. Typically, adsorption volume of solution was 50 mL and 50 mg Mγ-Fe_2O_3/CSCs were used in each adsorption. At given time intervals, the suspension containing adsorbents was extracted and adsorbents were collected using an adscititious magnet. MO concentration in supernate after magnetic separation was monitored by Cary 50 Model UV–vis spectrophotometer at λ_{max} = 464.9 nm. The amount of adsorption q_t (mg g^{-1}) was calculated from the change in MO concentration according to the following equation:

$$q_t = \frac{(C_0 - C)V}{W} \quad (1)$$

where C_0 is initial MO concentration (mg L^{-1}), C is the instantaneous MO concentration (mg L^{-1}), W is the weight of the adsorbent used (g), and V is the volume of solution (L).

The removal of MO (η) was calculated using the following equation:

$$\eta\% = \frac{(C_0 - C)}{C_0} 100 \quad (2)$$

3. Results and discussion

3.1. Characterization

3.1.1. XRD analysis

X-ray diffraction (XRD) is an effective method to investigate the existence of intercalation in composites. XRD patterns of chitosan (a), 1:10 Mγ-Fe_2O_3/CSCs (b), 2:5 Mγ-Fe_2O_3/CSCs (c) and magnetic γ-Fe_2O_3 nanoparticles (d) are shown in Fig. 2. Diffraction peaks of magnetic γ-Fe_2O_3 nanoparticles at 2θ of 30.26°, 35.64°, 43.34°, 53.84°, 57.36° and 62.96° corresponded to (2 2 0), (3 1 1), (4 0 0), (4 2 2), (5 1 1) and (4 4 0) lattice planes of γ-Fe_2O_3 (Fig. 2d), which was consistent with the database of maghemite (γ-Fe_2O_3) (JCPDS no. 39-1346) [23,24]. According to the Scherrer's equation, calculated average crystallite size of magnetic γ-Fe_2O_3 nanoparticles was about 25 nm. The diffraction spectrum of chitosan (Fig. 2a) did not find obvious crystalline peaks at the scan range 25–75°. With the introduction of γ-Fe_2O_3, Mγ-Fe_2O_3/CSCs samples showed typical diffraction peaks of γ-Fe_2O_3 (Fig. 2b and c) and the peaks of maghemite increased with the increase of γ-Fe_2O_3 dosage. Therefore, γ-Fe_2O_3 has been introduced into Mγ-Fe_2O_3/CSCs and kept intrinsic phase of maghemite. At the same time, the maghemite peaks in XRD patterns shifted slightly to lower angles compared

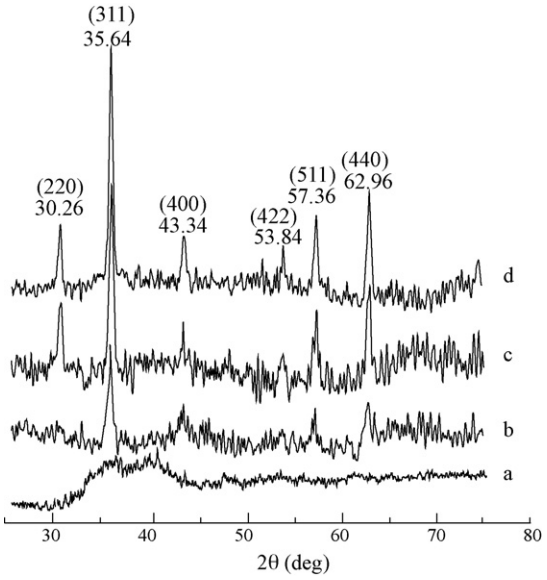

Fig. 2. XRD patterns of chitosan (a), 1:10 Mγ-Fe_2O_3/CSCs (b), 2:5 Mγ-Fe_2O_3/CSCs (c) and magnetic γ-Fe_2O_3 nanoparticles (d).

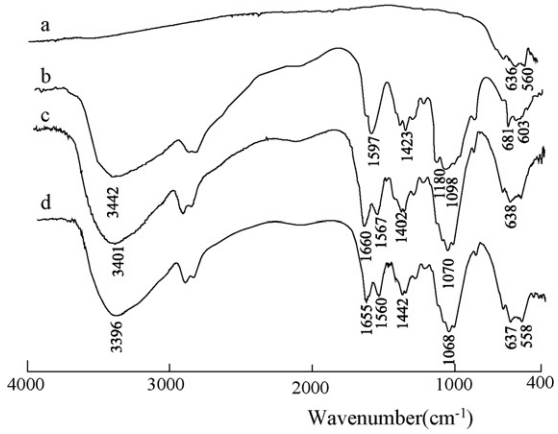

Fig. 3. FT-IR spectra of magnetic γ-Fe_2O_3 nanoparticles (a), raw chitosan (b), 1:10 Mγ-Fe_2O_3/CSCs (c) and 2:5 Mγ-Fe_2O_3/CSCs (d).

with those of magnetic γ-Fe_2O_3 nanoparticles, indicating that the interaction between chitosan and γ-Fe_2O_3 has occurred.

3.1.2. FT-IR analysis

Fig. 3 shows the FT-IR spectra of magnetic γ-Fe_2O_3 nanoparticles (a), chitosan (b), 1:10 Mγ-Fe_2O_3/CSCs (c) and 2:5 Mγ-Fe_2O_3/CSCs. For magnetic γ-Fe_2O_3 nanoparticles (Fig. 3a), peaks at 560 cm^{-1} and 636 cm^{-1} related to Fe–O group [21]. The strong absorption peak of chitosan (Fig. 3b) at 1597 cm^{-1} was assigned to the characteristic peak of NH_2, indicating that raw chitosan possessed high degree of deacetylation. While the spectra of 1:10 Mγ-Fe_2O_3/CSCs and 2:5 Mγ-Fe_2O_3/CSCs (Fig. 3c and d) displayed a disappearance of the peak at 1597 cm^{-1} and the formation of a new peak at 1655–1560 cm^{-1} was related to consumption of $-NH_2$ groups to form Schiff base [25,26]. Compared with the spectrum of chitosan (Fig. 3b), the spectra of two Mγ-Fe_2O_3/CSCs showed broader band at 3150–3700 cm^{-1}, which was attributed to hydroxyl (OH) stretching [27]. At the same time, its intensity decreased and the peak shifted from 3442 cm^{-1} (Fig. 3b) to lower wavenumber 3401 cm^{-1} (Fig. 3c) and 3396 cm^{-1} (Fig. 3d) with increasing dosage of γ-Fe_2O_3. This change suggested that γ-Fe_2O_3 was enwrapped by the interaction between chitosan and γ-Fe_2O_3 nanoparticles.

3.1.3. TG analysis

Typical TG and DSC curves of samples are depicted in Fig. 4. The TG curve of magnetic γ-Fe_2O_3 nanoparticles showed that weight loss over temperature ranges from 25 to 780 °C was about 1.36%, indicating that no significant weight loss took place (Fig. 4 left a). However, there was an obvious exothermic peak at 626 °C in the DSC curve of magnetic γ-Fe_2O_3 (Fig. 4 right a), representing a phase transition from γ-Fe_2O_3 to α-Fe_2O_3 [28]. The TG and DSC curves of two Mγ-Fe_2O_3/CSCs samples demonstrated similar trends. Firstly, two weight losses were observed at 25–780 °C. The first stage of weight loss occurred at 27–150 °C was due to evaporation of water physically adsorbed on the composites [29] and obvious endothermic peaks could be seen from corresponding DSC curves (Fig. 4 right b and c). The weight loss in second stage between 150 °C and 780 °C were 47.5% and 56.7% for 2:5 Mγ-Fe_2O_3/CSCs (Fig. 4 left b) and 1:10 Mγ-Fe_2O_3/CSCs (Fig. 4 left c), respectively, which were mainly due to the decomposition of polymer matrix in the Mγ-Fe_2O_3/CSCs [30]. To our surprise, there was no phase transition peak of nanosized Fe_2O_3 (Fig. 4 right b and c), which indicated that magnetic γ-Fe_2O_3 in the Mγ-Fe_2O_3/CSCs presented much more stable due to interaction between γ-Fe_2O_3 and chitosan.

3.1.4. SEM analysis

Morphology of samples was investigated using SEM. Fig. 5 presents typical SEM micrographs of crosslinked chitosan (Fig. 5a) and 1:10 Mγ-Fe_2O_3/CSCs (Fig. 5b). Obviously, the SEM micrograph of crosslinked chitosan presented relatively compact surface and some macropores. However, with the introduction of magnetic γ-Fe_2O_3 nanoparticles into chitosan by microemulsion process, there were significant changes on the surface morphology of Mγ-Fe_2O_3/CSCs (Fig. 5b). The SEM micrograph of Mγ-Fe_2O_3/CSCs (Fig. 5b) indicated that the composite adsorbent was composed of abound unequal microparticles with rough 2–10 μm outer

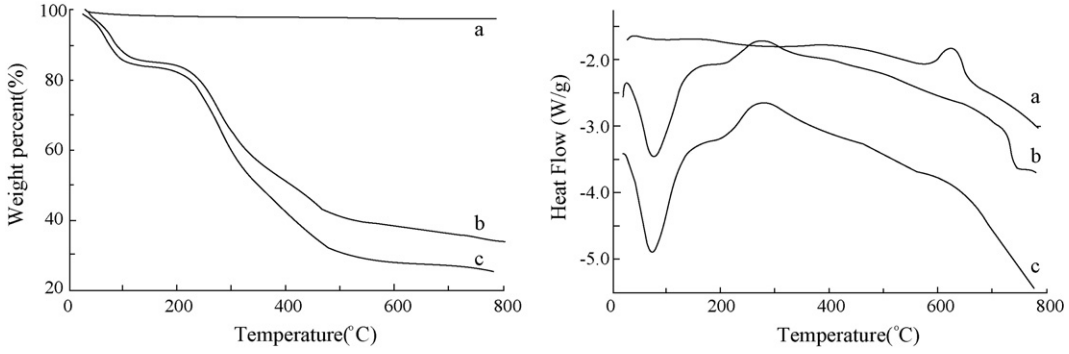

Fig. 4. TG (left) and DSC (right) curves of magnetic γ-Fe_2O_3 nanoparticles (a) 2:5 Mγ-Fe_2O_3/CSCs (b) and 1:10 Mγ-Fe_2O_3/CSCs (c).

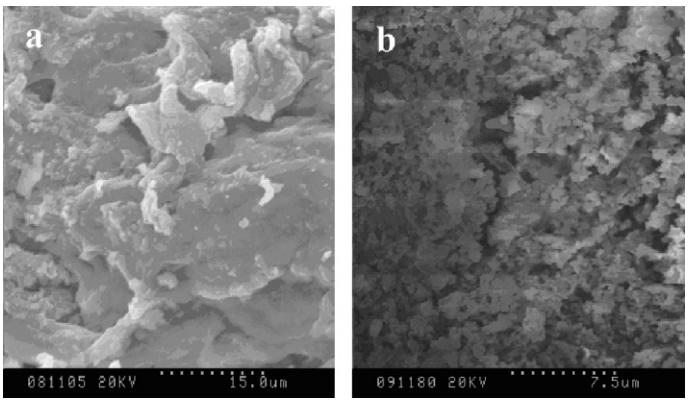

Fig. 5. SEM micrographs for crosslinked chitosan (a) and 1:10 Mγ-Fe_2O_3/CSCs (b).

diameters. The particle size of Mγ-Fe_2O_3/CSCs was much bigger than that of magnetic γ-Fe_2O_3 nanoparticles (20–30 nm), indicating that γ-Fe_2O_3 has been encapsulated by chitosan. This was in agreement with the XRD results. Mγ-Fe_2O_3/CSCs provided a larger surface and smaller particle diameter compared with crosslinked chitosan, which offered advantageous condition for the adsorption of azo dyes from solution onto the novel composite adsorbent.

3.1.5. Magnetic separation property of Mγ-Fe_2O_3/CSCs

Hysteresis loops of 1:10 Mγ-Fe_2O_3/CSCs and 2:5 Mγ-Fe_2O_3/CSCs were measured in fields between ±1.5 kOe at room temperature and the results are shown in Fig. 6a. The saturated magnetization ($\sigma_{s,1}$) of 2:5 Mγ-Fe_2O_3/CSCs reached at 4.36 emu g^{-1} and the saturated magnetization ($\sigma_{s,2}$) of 1:10 Mγ-Fe_2O_3/CSCs was 1.44 emu g^{-1}. The ratio of $\sigma_{s,1}$:$\sigma_{s,2}$ was 3.1:1, which was almost consistent with the ratio (3.0:1) of γ-Fe_2O_3 content in two Mγ-Fe_2O_3/CSCs samples. The result indicated that magnetic γ-Fe_2O_3 nanoparticles enwrapped by crosslinked chitosan kept their intrinsic magnetic properties and crystal structure. Therefore, the saturated magnetization (σ_s) of Mγ-Fe_2O_3/CSCs could be expediently adjusted by changing additive dosage of γ-Fe_2O_3. In order to verify magnetic separation of Mγ-Fe_2O_3/CSCs, an adscititious magnet was used to separate the adsorbents from mixture solution. Fig. 6b showed that Mγ-Fe_2O_3/CSCs dispersed well in water before magnetic separation, providing good condition and more surface for MO adsorption on Mγ-Fe_2O_3/CSCs. However, magnetic composite adsorbents could be quickly collected and immobilized on the bottom of test tube near the magnet in 10 s by applying an adscititious magnetic field (Fig. 6c). Therefore, Mγ-Fe_2O_3/CSCs could

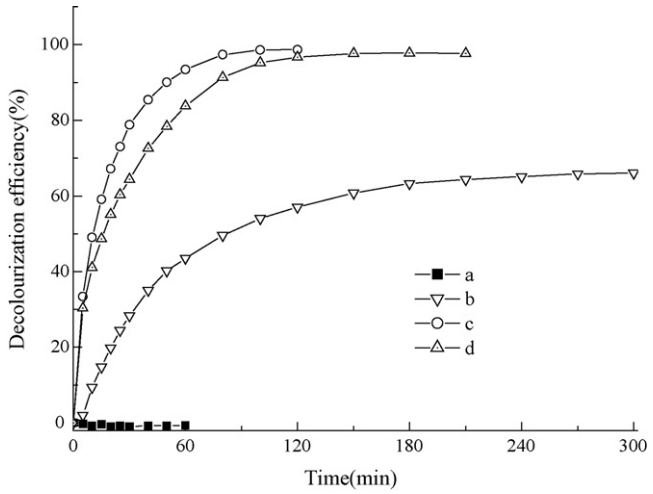

Fig. 7. Adsorption of MO on magnetic γ-Fe_2O_3 nanoparticles (a), crosslinked chitosan (b), 1:10 Mγ-Fe_2O_3/CSCs (c) and 2:5 Mγ-Fe_2O_3/CSCs (d). Experimental conditions: initial MO concentration 30 mg L^{-1}; adsorbent dosage 1.0 g L^{-1}; temperature 27 ± 0.2 °C; stirring rate 100 rpm.

easily be separated and recovered from the adsorption system by a simple magnetic process after adsorption.

3.2. Adsorption property

3.2.1. Comparison of MO adsorption with different adsorbents

Fig. 7 shows adsorption percent of MO as a function of contact time onto four different adsorbents, namely magnetic γ-Fe_2O_3 nanoparticles (a), crosslinked chitosan (b), 1:10 Mγ-Fe_2O_3/CSCs (c) and 2:5 Mγ-Fe_2O_3/CSCs (d), respectively. The saturation adsorption capacities of MO onto magnetic γ-Fe_2O_3 nanoparticles, crosslinked chitosan, 1:10 Mγ-Fe_2O_3/CSCs and 2:5 Mγ-Fe_2O_3/CSCs were measured as 0.10 mg g^{-1}, 20.10 mg g^{-1}, 29.50 mg g^{-1} and 29.37 mg g^{-1}, respectively. Two Mγ-Fe_2O_3/CSCs adsorbents showed higher adsorption capacities as compared with those of magnetic γ-Fe_2O_3 nanoparticles and crosslinked chitosan. On one hand, nanoparticles embedded in biopolymer materials expanded adsorption capacity due to the improvement in the electrostatic interaction [31]. On the other hand, with the introduction of γ-Fe_2O_3, Mγ-Fe_2O_3/CSCs provided more available sites for MO adsorption due to a larger surface and smaller pore diameter compared with crosslinked chitosan. This phenomenon has been proved by the result of SEM analysis.

At the same time, it took 100 min, 150 min and 270 min to attain equilibrium for 1:10 Mγ-Fe_2O_3/CSCs, 2:5 Mγ-Fe_2O_3/CSCs and crosslinked chitosan, respectively. The MO removal increased

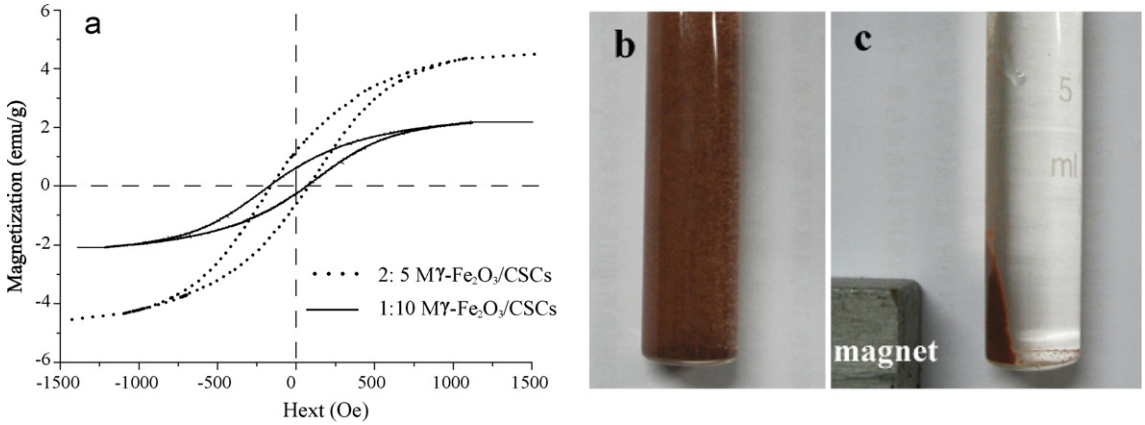

Fig. 6. Magnetization curves (a) of Mγ-Fe_2O_3/CSCs and photographs of adsorption system before (b) and after (c) magnetic separation.

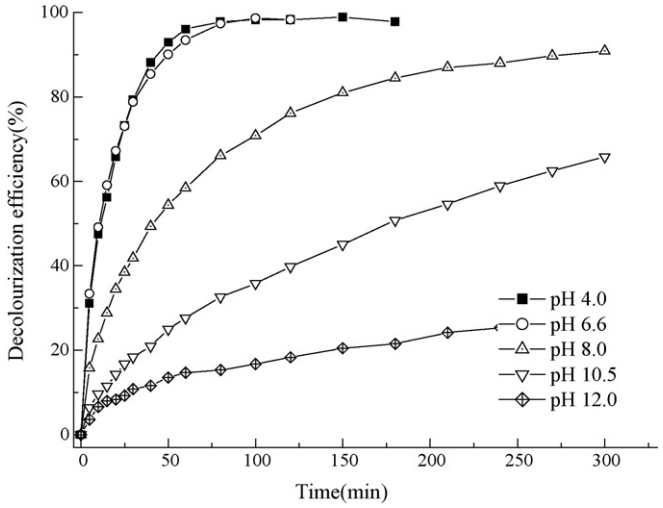

Fig. 8. Effect of initial solution pH on the adsorption of MO by 1:10 Mγ-Fe_2O_3/CSCs. Experiment conditions: initial MO concentration 30 mg L^{-1}; adsorbent dosage 1.0 g L^{-1}; pH range 4.0–12.0; temperature 27 ± 0.2 °C; stirring rate 100 rpm.

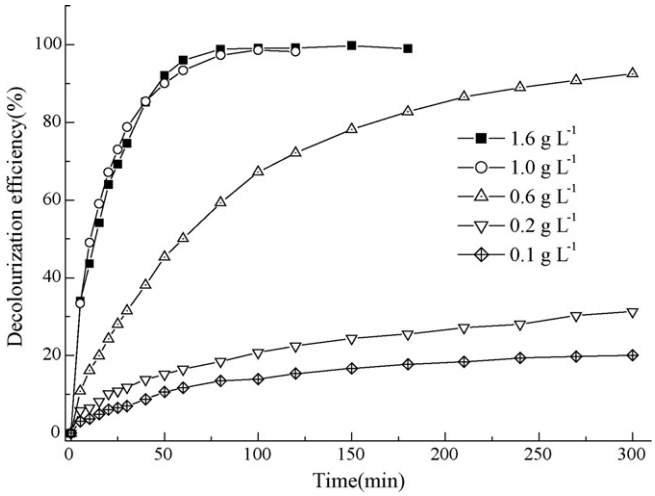

Fig. 9. Effect of adsorption dosage on MO adsorption by 1:10 Mγ-Fe_2O_3/CSCs. Experiment conditions: initial MO concentration 30 mg L^{-1}; adsorbent dosage range 0.1–1.6 g L^{-1}; initial solution pH 6.6; temperature 27 ± 0.2 °C; stirring rate 100 rpm.

dramatically and the adsorption equilibrium was achieved much faster with the introduction of nanosized γ-Fe_2O_3. It indicated that the adsorption capacity of Mγ-Fe_2O_3/CSCs towards MO was better than both bottom ash and de-oiled soya in previous research [32]. Therefore, considering relatively low cost and rapid adsorption rate of the composite adsorbent, it could be used as a promising alternative adsorbent to decolor the dye effluent.

3.2.2. Effect of initial pH

The solution pH is one of the dominant parameters affecting the adsorption of organic dyes onto solid polymeric adsorbent [33]. Effect of initial solution pH on MO adsorption by 1:10 Mγ-Fe_2O_3/CSCs at 27 ± 0.2 °C was investigated for 30 mg L^{-1} MO solution and the results are illustrated in Fig. 8. The effect of pH on MO adsorption was remarkable in our experimental conditions. As seen from Fig. 8, adsorption percent of MO onto 1:10 Mγ-Fe_2O_3/CSCs decreased from 98.27% to 39.80% after 120 min adsorption with a decrease in pH from 4.0 to 12.0. This result indicated that the adsorption capacity decreased with the increase of initial solution pH. The similar effect of pH on MO adsorption was observed in other researches [32,34]. Chitosan has a positively charged surface below pH 6.5 (point of zero potential). In acidic solution, hydrogen atoms (H^+) in solution can protonate amine groups (–NH_2) of chitosan [35]. As a result, the electrostatic interactions between MO anions and chitosan with positively charged surface increased in acidic solution.

3.2.3. Effect of adsorbent amount

Adsorption dosage is another important parameter because it determines the capacity of an adsorbent for a given initial concentration of adsorbate. Effect of adsorbent dosage was studied on MO removal from aqueous solutions by varying the amount of 1:10 Mγ-Fe_2O_3/CSCs from 0.10 g L^{-1} to 1.6 g L^{-1} while keeping other parameters constant such as 30 mg L^{-1} initial dye concentration, initial solution pH 6.6 and stirring rate 100 rpm. Color removal of MO increased from 15.35% to 98.25% with increasing adsorbent dosage from 0.1 g L^{-1} to 1.0 g L^{-1} (Fig. 9). Available active sites increased with the increase of adsorbent dosage. However, further increase in adsorbent dosage to 1.6 g L^{-1} only leads to the adsorption percent increase by 0.94%. At the same time, the amount adsorbed per unit mass of MO decreased evidently from 29.46 mg g^{-1} to 18.70 mg g^{-1}. The decrease in the amount adsorbed of MO (q_t) with increasing adsorbent dosage was due to unsaturated adsorption active sites during the adsorption process. As a result, 1.0 g L^{-1} was the optimum adsorbent dosage for MO adsorption onto 1:10 Mγ-Fe_2O_3/CSCs.

3.2.4. Adsorption kinetics

Adsorption kinetics is one of the most important characters which govern the solute uptake rate and represent adsorption efficiency of adsorbent for design operation and optimization [36]. To investigate adsorption kinetics of MO on different adsorbents, three different kinetic models, i.e. Lagergren-first-order model, pseudo-second-order kinetic model and intraparticle diffusion model were used to fit the adsorption kinetic data.

The Lagergren-first-order kinetic, pseudo-second-order kinetic model and intraparticle diffusion model can be given by Eqs. (3)–(5) [37].

$$q_t = q_e \left(1 - \frac{t}{10^{(k_1/2.303)^t}}\right) \quad (3)$$

$$q_t = \frac{k_2 q^2 t}{1 + k_2 q_e t} \quad (4)$$

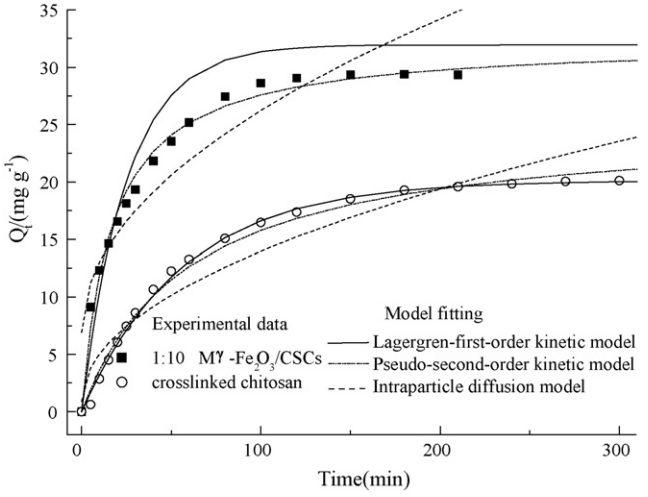

Fig. 10. Adsorption kinetics of MO on crosslinked chitosan and 1:10 Mγ-Fe_2O_3/CSCs. Experimental conditions: initial MO concentration 30 mg L^{-1}; adsorbent dosage 1.0 g L^{-1}; temperature 27 ± 0.2 °C; stirring rate100 rpm.

Table 1
Kinetic parameters of MO adsorption onto adsorbents for 30 mg L^{-1} initial dye concentration.

Adsorbents	$q_{e,exp}$ (mg g^{-1})	Lagergren-first-order kinetic model			Pseudo-second-order kinetic model			Intraparticle mass transfer diffusion model		
		$q_{e,cal}$ (mg g^{-1})	k_1 (min^{-1})	R^2	$q_{e,cal}$ (mg g^{-1})	k_2 (g mg^{-1} min^{-1})	R^2	k_i (mg g^{-1} $min^{-1/2}$)	c (mg g^{-1})	R^2
Crosslinked chitosan	20.10	20.12	0.00758	0.998	25.17	0.003669	0.992	1.47	0.01	0.932
1:10 Mγ-Fe_2O_3/CSCs	29.49	26.83	0.02194	0.991	32.06	0.000338	0.999	2.10	7.01	0.938

$$q_t = k_i t^{1/2} + c \quad (5)$$

where q_e and q_t are the amounts of MO (mg g^{-1}) adsorbed on adsorbent at equilibrium and at a given time t (min), respectively; k_1 is the rate constant (min^{-1}) of Lagergren-first-order kinetic model, k_2 is the rate constant (g mg^{-1} min^{-1}) of pseudo-second-order kinetic mode, and k_i is the intraparticle diffusion rate constant (mg g^{-1} $min^{-1/2}$); c (mg g^{-1}) is the intercept of intraparticle diffusion model. Values of c give information about the thickness of the boundary layer, i.e. the larger intercept the greater is the boundary layer effect.

The regression plots of Lagergren-first-order kinetic model, pseudo-second-order kinetic model and intraparticle diffusion model are shown in Fig. 10 and the corresponding adsorption rate constants are summarized in Table 1. The validity of each model is checked by the correlation coefficient (R^2) as well as the experimental and calculated data. For MO adsorption on crosslinked chitosan, the correlation coefficient (R^2 = 0.998) of Lagergren-first-order kinetic model was higher than that of pseudo-second-order kinetic model (R^2 = 0.992). What is more, the calculated equilibrium adsorption capacity $q_{e,cal}$ (20.12 mg g^{-1}) agreed better with the experimental value $q_{e,exp}$ (20.10 mg g^{-1}) for Lagergren-first-order kinetic model (Table 1). Therefore, the kinetic data of MO adsorption on crosslinked chitosan fitted Lagergren-first-order kinetic model better than pseudo-second-order kinetic model. However, the correlation coefficients (R^2) of the Lagergren-first-order and pseudo-second-order kinetic models were 0.991 and 0.999 for MO adsorption on 1:10 Mγ-Fe_2O_3/CSCs, respectively, indicating that the pseudo-second-order kinetic model was more valid to predict the behavior of MO adsorption. This supported the assumption of the model that the adsorption was due to chemisorption. High correlations for pseudo-second-order kinetic equation for dyes adsorption on various poriferous adsorbents have also been reported [31,38] and Lagergren-first-order kinetic equation would be applicable only over the initial stage of the adsorption process on poriferous adsorbents [39].

The adsorbate can be transferred from the solution phase to the surface of adsorbent in several steps. The steps might include external diffusion, pore diffusion, surface diffusion and adsorption on the pore surface. According to Eq. (5), the intraparticle diffusion rate constants were calculated from the plots of q_t versus $t^{0.5}$ for crosslinked chitosan and 1:10 Mγ-Fe_2O_3/CSCs. The regression analysis showed that the correlation coefficient values (R^2) over the whole time range were lower than 0.94, indicating that more than one process affected the MO adsorption on both crosslinked chitosan and 1:10 Mγ-Fe_2O_3/CSCs [40]. For MO adsorption on crosslinked chitosan, the c value of intraparticle diffusion model was 0.01 mg g^{-1}, indicating that intraparticle diffusion was the rate-controlling step. For MO adsorption on 1:10 Mγ-Fe_2O_3/CSCs, the large c value (7.01 mg g^{-1}) suggested that intraparticle diffusion was not the rate-controlling step and the boundary layer diffusion controlled the adsorption to some degree. With the introduction of γ-Fe_2O_3 nanopartilces, 1:10 Mγ-Fe_2O_3/CSCs provided a larger surface and smaller particle diameter, resulting in more available adsorption active sites on the surface of 1:10 Mγ-Fe_2O_3/CSCs, compared with crosslinked chitosan. Therefore the boundary layer diffusion of solute molecules had important effect on MO adsorption on 1:10 Mγ-Fe_2O_3/CSCs. This result was in agreement with the SEM analysis.

4. Conclusions

Magnetic nanosized γ-Fe_2O_3/crosslinked chitosan composites (Mγ-Fe_2O_3/CSCs) were prepared by microemulsion process using magnetic γ-Fe_2O_3 nanoparticles as magnetic material and chitosan as basic adsorbent, then characterized by XRD, FT-IR, TGA, DSC, SEM and VSM. The characterizations' results indicated that magnetic γ-Fe_2O_3 nanoparticles have been successfully introduced into the composites and kept intrinsic magnetic properties. The magnetic properties of Mγ-Fe_2O_3/CSCs could be expediently adjusted by changing additive γ-Fe_2O_3 dosage. The Mγ-Fe_2O_3/CSCs adsorbents exhibited faster adsorption rate towards methyl orange compared with crosslinked chitosan. After adsorption, the Mγ-Fe_2O_3/CSCs could be effectively separated from reaction solution in 10 s by applying an adscititious magnetic field. With the introduction of γ-Fe_2O_3, both transports of MO from aqueous solution through the particle interfaces into pores and adsorption on adsorbent surface available were responsible for MO adsorption on Mγ-Fe_2O_3/CSCs. Both effects of initial pH and adsorbent dosage on MO adsorption were remarkable in experimental conditions.

Acknowledgements

The authors wish to acknowledge the financial support of the research by Specialized Research Fund for the Bairen Program of Taizhou University (no. TZUDF 2007-167). Special thanks to Mr. Guping Wang and Mrs. Fang Wang for technical support during XRD measurements and TG measurements in this work, respectively.

References

[1] Y. Badr, M.A. Mahmoud, Photocatalytic degradtion of methyl orange by gold silver nono-core/Silica nano-shell, J. Phys. Chem. Solids 68 (2007) 413–419.
[2] L.C. Chen, Effects of factors and interacted factors on the optimal decolorization process of methyl orange by ozone, Water Res. 34 (2000) 974–982.
[3] T. Robinson, B. Chandran, P. Nigam, Removal of dyes from a synthetic textile dye effluent by biosorption on apple pomace and wheat straw, Water Res. 36 (2002) 2824–2830.
[4] X.J. Lu, B. Yang, J.H. Chen, R. Sui, Treatment of wastewater containing azo dye reactive brilliant red X-3B using sequential ozonation and upflow biological aerated filter process, J. Hazard. Mater. 161 (2009) 234–241.
[5] Y.J. Li, X.D. Li, J.W. Li, J. Yin, Photocatalytic degradation of methy orange by TiO_2-coated activated barbon and kinetic study, Water Res. 40 (2006) 1119–1126.
[6] H.Y. Zhu, R. Jiang, L. Xiao, Y.H. Chang, Y.J. Guan, X.D. Li, G.M. Zeng, Photocatalytic decolorization and degradation of Congo Red on innovative crosslinked Chitosan/nano-CdS composite catalyst under visible light irradiation, J. Hazard. Mater. 169 (2009) 933–940.
[7] R. Jiang, H.Y. Zhu, X.D. Li, L. Xiao, Visible light photocatalytic decolourization of C. I. Acid Red 66 by chitosan capped CdS composite nanoparticles, Chem. Eng. J. 152 (2009) 537–542.
[8] J.H. Qu, Research progress of novel adsoprtion processes in water purification:a review, J. Environ. Sci. 20 (2008) 1–13.
[9] S.Y. Mak, D.H. Chen, Fast adsorption of methylene blue on polyacrylic acid-cound iron oxide magnetic nanoparticles, Dyes Pigments 61 (2004) 93–98.
[10] G. Crini, P.M. Badot, Application of chitosan, a natural aminopolysaccharide, for dye removal from aqueous solutions by adsorption processes using batch studies: a review of recent literature, Prog. Polym. Sci. 33 (2008) 399–447.
[11] M.S. Chiou, H.Y. Li, Equilibrium and kinetic modeling of adsorption of reactive dye on cross-linked chitocan beads, J. Hazard. Mater. 93 (2002) 233–248.
[12] L. Wang, A.Q. Wang, Adsorption properties of congo red from aqueous solution onto N,O-carboxymethly- chitosan, Bioresour. Technol. 99 (2008) 1043–1048.

[13] Z.G. Hu, J. Zhang, W.L. Chan, Y.S. Szeto, The sorption of acid dye onto chitosan nanoparticles, Polymer 47 (2006) 5838–5842.
[14] J.L. Gong, B. Wang, G.M. Zeng, C.P. Yang, C.G. Niu, Q.Y. Niu, W.J. Zhou, Y. Liang, Removal cationic dyes from aqueous solution using magnetic multi-wall carbon nanotube nanocomposite as adsorbent, J. Hazard. Mater. 164 (2009) 1517–1522.
[15] X.J. Peng, Z.K. Luan, Z.C. Di, Z.G. Zhang, C.L. Zhu, Carbon nanotubes-iron oxides magnetic composites as adsorbent for removal of Pb(II) and Cu(II) from water, Carbon 43 (2005) 855–894.
[16] C.L. Chen, J. Hu, D.D. Shao, J.X. Li, X.K. Wang, Adsorption behavior of multiwall carbon nanutube/iron oxide magnetic composites for Ni(II) and Sr (II), J. Hazard. Mater. 164 (2009) 923–928.
[17] T. Tuutijärvi, J. Lu, M. Sillanpää, G. Chen, As(V) adsorption on maghemite nanoparticles, J. Hazard. Mater. 166 (2009) 1415–1420.
[18] A.P. Zhu, L.H. Yuan, T.Q. Liao, Suspension of Fe_3O_4 nanoparticles stabilized by chitosan and O-carboxymethyl chitosan, Int. J. Pharm. 350 (2008) 361–368.
[19] Y. Wu, Y.J. Wang, G.S. Luo, Y.Y. Dai, In situ preparation of magnetic Fe_3O_4-chitosan nanoparticles for lipase immobilization by cross-linking and oxidation in aqueous solution, Bioresour. Technol. 100 (2009) 3459–3464.
[20] Y.C. Chang, D.H. Chen, Preparation and adsorption properties of monodisperse chitosan-bound Fe_3O_4 magnetic nanoparticles for removal of Cu(II) ions, J. Colloid Interface Sci. 283 (2005) 446–451.
[21] G.Y. Li, Y.R. Jiang, K.L. Huang, P. Ding, L.L. Yao, Kinetics of adsorption of *Saccharomyces cerevisiae* mandelated dehydrogenase on magnetic Fe_3O_4-chitosan nanoparticle, Colloids Surf., A 320 (2008) 11–18.
[22] G.Y. Li, Y.R. Jiang, K.L. Huang, P. Ding, J. Chen, Preparation and properties of magnetic Fe_3O_4-chitosan nanoparticle, J. Alloys compd. 466 (2008) 451–456.
[23] S.W. Cao, Y.J. Zhu, Y.P. Zeng, Formation of γ-Fe_2O_3 hierarchical nanostructures at 500 °C in high magnetic field, J. Magn. Magn. Mater. 321 (2009) 3057–3060.
[24] Z.H. Jing, Synthesis, characterization and gas sensing properties of undoped and Zn-doped Fe_2O_3-based gas sensors, Mater. Sci. Eng., A 441 (2006) 176–180.
[25] J. Brugnerotto, J. Lizardi, F.M. Goycoolea, W.A. Monal, J. Desbrières, M. Rinaudo, An infrared investigation in relation with chitin and chitosan characterization, Polymer 42 (2001) 3569–3580.
[26] A. Pawlak, M. Mucha, Thermogravimetric and FTIR studies of chiotsan blends, Thermochim. Acta 396 (2003) 153–166.
[27] Y. Hu, Y.M. Du, J.H. Yang, J.F. Kennedy, X.H. Wang, L.S. Wang, Synthesis, characterization and antibacterial activity of guanidinylated chitosan, Carbohydr. Polym. 67 (2007) 66–72.
[28] T.S. Zhang, H.M. Luo, H.X. Zeng, R.F. Zhang, Y.S. Shen, Synthesis and gas sensing characteristics of high thermostability γ-Fe_2O_3 powder, Sens. Actuators B 32 (1996) 181–184.
[29] Z.H. Jing, Y. Wang, S.H. Wu, Preparation and gas sensing properties of pure and dopped γ-Fe_2O_3 by an anhydrous solvent method, Sens. Actuators, B 113 (2006) 177–181.
[30] K. Sunderland, P. Brunetti, L. Spinu, J.Y. Fang, Z.J. Wang, W.G. Lu, Synthesis of γ-Fe_2O_3/polypyrrodle nanocomposite materials, Mater. Lett. 58 (2004) 3136–3140.
[31] X.G. Luo, L.N. Zhang, High effect adsorption of organic dyes on magnetic cellulose beads entrapping activated carbon, J. Hazard. Mater. 171 (2009) 340–347.
[32] A. Mittal, A. Malviya, D. Kaur, J. Mittal, L. Kurup, Studies on the adsorption kinetics and isotherms for the removal and recovery of Methyl Orange from wastewaters using waste materials, J. Hazard. Mater. 148 (2007) 229–240.
[33] M. Doğan, H. Abak, M. Alkan, Adsorption of methylene blue onto hazelnut shell: Kinetics, mechanism and activation parameters, J. Hazard. Mater. 164 (2009) 177–181.
[34] S.C.S. Chatterjee, B.P. Chatterjee, A.R. Das, A.K. Guha, Adsorption of a model anionic dye, eosin Y, from aqueous solution by chitosan hydrobeads, J. Colloid Interface Sci. 288 (2005) 30–35.
[35] N. Sakkayawong, P. Thiravetyan, W. Nakbanpote, Adsorption mechanism of synthetic reactive dye wastewater by chitosan, J. Colloid Interface Sci. 286 (2005) 36–42.
[36] G.C. Chen, X.Q. Shan, Y.Q. Zhou, X.E. Shen, H.L. Huang, S.U. Khan, Adsorption kinetics, isotherms and thermodynamics of atrazine on surface oxidized multiwalled carbon nanotubes, J. Hazard. Mater. 169 (2009) 912–918.
[37] C.H. Weng, C.Z. Tsai, S.H. Chu, Y.C. Sharma, Adsorption characteristics of copper(II) onto spent activated clay, Sep. Purif. Technol. 54 (2007) 187–197;
C.H. Weng, Y.F. Pan, Adsorption of a cationic dye (methylene blue) onto spent activated cay, J. Hazard. Mater. 144 (2007) 355–362.
[38] E. Demirbas, N. Dizge, M.T. Sulak, M. Kobya, Adsorption kinetics and equilibrium of copper from aqueous solutions using hazelnut shell activated carbon, Chem. Eng. J. 148 (2009) 480–487.
[39] Y.S. Ho, G. Mckay, The sorption of Lead(II) ions on peat, Water Res. 33 (1999) 578–584.
[40] W.H. Cheung, Y.S. Szeto, G. McKay, Intraparticle diffusion processes during acid dye adsorption onto chitosan, Bioresour. Technol. 98 (2007) 2897–2904.